Electronic Materials Letters
https://doi.org/10.1007/s13391-023-00483-8

ORIGINAL ARTICLE - ENERGY AND SUSTAINABILITY

Improved Catalytic Properties of Fluorine-Doped $La_{0.6}Sr_{0.4}Co_{0.2}Fe_{0.8}O_{3-\delta}$ for Air Electrode with High-Performance Metal-Air Batteries

Jiyoun Kim[1,2] · Jeongah Lee[1] · Sangwoo Kim[1] · WooChul Jung[1]

Received: 15 December 2023 / Accepted: 29 December 2023

Abstract

$La_{0.6}Sr_{0.4}Co_{0.2}Fe_{0.8}O_{3-\delta}$ (LSCF), a perovskite material, is widely recognized as an excellent catalyst for the oxygen evolution reaction (OER). An anion doping strategy was implemented to enhance the presence of highly oxidation-active O^{2-}/O^{-} species crucial for the electrochemical reaction, effectively replacing oxygen. The introduction of 5 mol% fluorine to LSCF resulted in improved OER performance, comparable to that of commercial noble catalysts. Furthermore, we confirmed that fluorine-doped LSCF enhanced the oxygen reduction reaction (ORR) performance, establishing its effectiveness as a bifunctional catalyst. Moreover, when utilized as an air electrode in a homemade zinc-air battery cell, the electrochemical performance of the doped LSCF remained stable after repeated charge/discharge tests. These findings underscore the potential application of anion doping in electrochemical devices.

Graphical Abstract

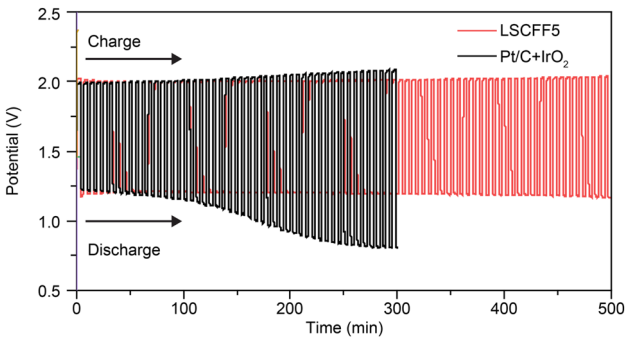

Keywords Perovskite · Bifunctional catalyst · Oxygen reduction reaction · Oxygen evolution reaction · Electrochemical devices

1 Introduction

Owing to escalating demand for green and sustainable energy sources, there is a significant focus on developing low-cost and efficient energy technologies. Metal–air batteries, composed of metal electrodes, oxygen electrodes, and electrolytes, are considered promising for various applications to meet future energy requirements [1, 2]. Compared to Li–ion batteries, Zn–air and Li–air batteries exhibit

✉ WooChul Jung
wcjung@kaist.ac.kr

[1] Department of Materials Science and Engineering, Korea Advanced Institute of Science and Technology, 291 Daehak-ro, Yuseong-gu, Daejeon 34141, Republic of Korea

[2] Materials & Energy Technology Center, Agency for Defense Development, Yuseong P.O. Box 35, Daejeon 34186, Republic of Korea

Published online: 31 January 2024

exceptionally high energy densities among rechargeable batteries. While Li–air batteries offer the highest theoretical specific energy of 11,140 Wh kg^{-1}, they face challenges with water sensitivity, the use of organic electrolytes, and technical and economic hurdles. On the other hand, Zn–air batteries, with a lower theoretical specific energy of 1084 Wh kg^{-1}, are more attractive due to their stable alkaline electrolytes that do not induce significant corrosion [3–5].

Despite these advantages, several key issues, including the kinetics of the oxygen evolution reaction (OER) and oxygen reduction reaction (ORR), low cyclic performance, and large overpotentials, need to be addressed for commercialization of Zn-air batteries. The efficiency of both ORR and OER is crucial for battery performance during discharge and charge, respectively [4–6]. However, developing catalysts suitable for both reactions is challenging due to significantly disparate reaction conditions regarding electrical potential. While Pt and Ir-oxide-based materials are commercially effective catalysts, their widespread application is hindered by production costs and scarcity. Therefore, developing transition metal-based catalysts with outstanding performance and relatively low cost is imperative.

Perovskite oxides (ABO_3), where A is a rare earth metal and B is a transition metal, are considered promising electrocatalysts for Zn-air batteries due to their high electronic and ionic conductivity and catalytic activity. Perovskite oxides have been explored as catalyst materials because the amount of saturated oxygen and conductivity can be easily controlled by partially replacing A- and B-cations [7]. An iron-rich perovskite, $La_{0.6}Sr_{0.4}Co_{0.2}Fe_{0.8}O_{3-\delta}$ (LSCF), is known for its decent OER/ORR performance and stability, attributed to the formation of a structurally disordered layer at the surface [8]. While some results of applying LSCF as a catalyst for room temperature devices have been reported, further investigation is required to enhance the catalytic properties and durability of the material for ORR/OER applications [8–10].

In parallel, while numerous research results have focused on the effects of A- and B-site cation doping in perovskite oxide, the doping of F, Cl, Br, and S anions at the oxygen position has garnered less attention compared to cation doping [11–13]. This less frequent exploration of anion doping has led to increased interest. Shao's group demonstrated that F doping in perovskite oxides could reduce the density of valency electrons of O^{2-} and decrease the chemical bonding energy between cations and anions, resulting in a remarkable improvement in oxygen mobility and permeability [12]. Li et al. also reported that F-doped $Sr_2Fe_{1.5}Mo_{0.5}O_{5.9}F_{0.1}$, as the Solid Oxide Electrolysis Cell (SOEC) cathode, exhibited enhanced catalytic performance for CO_2 reduction reactions, with increased surface oxygen species concentration, CO_2 adsorption, and bulk oxygen vacancy concentration [13]. Anion doping has been shown to positively impact physical properties related to catalytic properties, such as stability enhancement by controlling electronic structure, crystal structure, and oxygen movement through the addition of a small amount of dopant. Among them, F, with its strong electronegativity, when doped at an oxygen site, is known to weaken the bonding force between metal and oxygen, facilitating the release of oxygen from the lattice and creating a large number of active species for OER/ORR [14]. The O^{2-} site of perovskite oxide is partially substituted by F^- in the presence of F sources, and the M-F-M ligands reduces the transition metals while decreasing their electron valence. Simultaneously, oxygen ions on the surface are activated, inducing highly oxidizing O^{2-}/O^- species, which act as highly catalytic reactive sites for OER/ORR [15]. LSCF is well-known as a commercial material for fuel-cell electrodes and various electrochemical energy storage devices, and it has gained attention as a bifunctional catalyst for OER/ORR. However, the anion doping effect on LSCF with regard to OER/ORR at room temperature is not clarification thoroughly. In this study, F anions are selected as the anion dopant for oxygen to investigate the effect on OER/ORR. F dopant in oxygen sites affects the lattice structure and electrochemical performance of LSCF. In particular, the enlarged lattice volume and the weakened bond strength between oxygen and B-site metal increases the amount of electrochemically active species, which induces intensified OER/ORR performance and stability. Ultimately, the enhanced performance as an air electrode as evaluated with a cycle test shows that anion-doped LSCF can be a potential candidate for the bifunctional catalyst for Zn-air batteries.

2 Results and Discussion

To ascertain the structural changes in the final product, $La_{0.6}Sr_{0.4}Co_{0.2}Fe_{0.8}O_{3-x}F_x$ (LSCFF, x = 0, 0.01, 0.03, 0.05, 0.075, and 0.10), denoted as LSCFF00, LSCFF01, LSCFF03, LSCFF05, LSCFF075, and LSCFF10, powders were analyzed using X-ray diffraction (XRD) in the range of 20 to 80 degrees, as illustrated in Fig. 1a. The corresponding peaks indicate the successful formation of a single perovskite when x is below 0.5, consistent with the standard card (PDF# 74–2203). However, impurity peaks are observed when x is 0.075 or more, revealing the presence of SrF_2 (PDF#06–0262) in the powders. As the fluorine (F) content increases from 0 to 0.10, the highest peak (Fig. 1b) shifts slightly to a lower angle. TEM images (Fig. 1c) confirm that the intended elements (La, Sr, Co, Fe, O, F) are distributed homogeneously over the crystalline surface. The (110) peak of LSCFF05 is negatively shifted from 2θ=32.58° (of the pristine LSCF) to from 2θ=32.54°. The crystalline symmetry of the pristine and F-doped LSCF, refined with the space group I4/mmm (Table S1), is maintained as a tetragonal

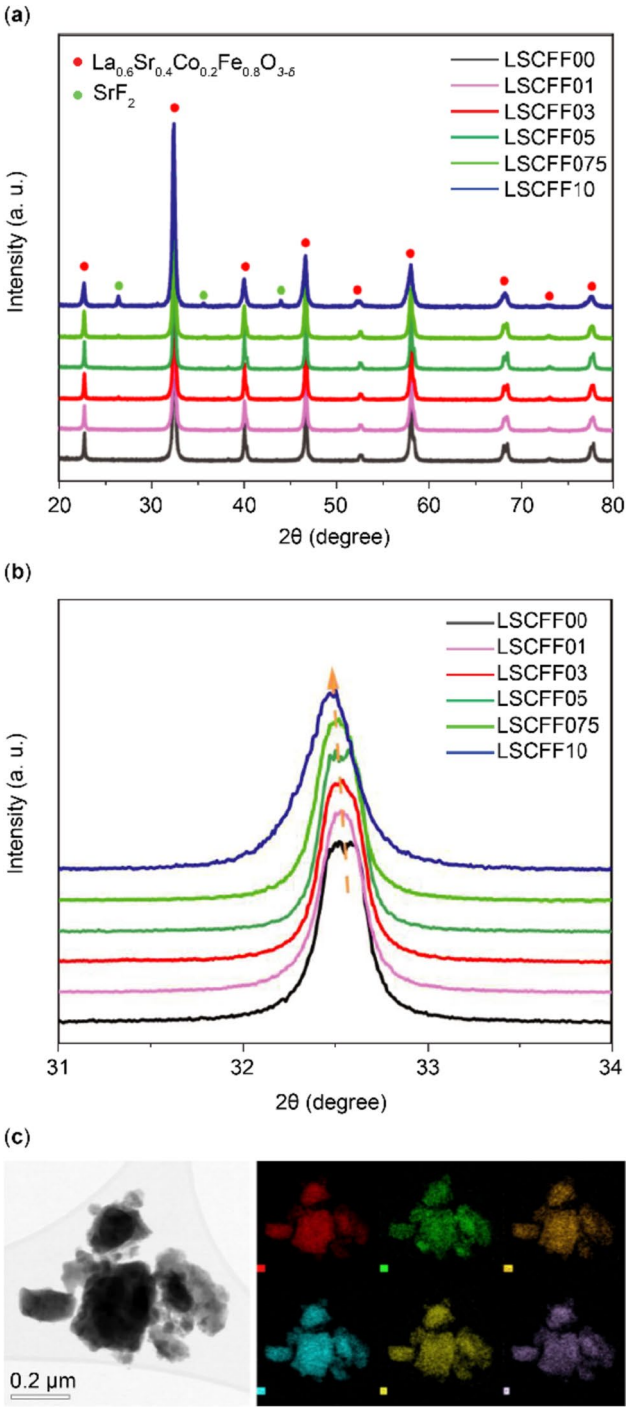

Fig. 1 Element and structural characteristics of LSCFF powders: **a** XRD patterns of LSCFF sintered at 950 °C in 20–80°, **b** enlarged XRD patterns of **a** at 31–34°, **c** STEM-EDX analysis results of LSCFF05

structure even after doping. This could be attributed to lattice expansions due to charge compensation induced by F doping, initiating the reduction of valence-changeable B-site cations rather than the oxidation of invariable A-site cations. Valence-negative-shifted metal cations exhibit a larger ionic radius than their more positive counterparts, increasing the distance between two neighboring M cations [14]. As displayed in Table S1, F doping increases the lattice parameters along the a, b, and c axes (with the c-axis parameter showing the greatest increase), resulting in volume expansion. Another probable reason for the crystalline expansion is the transformation of the $Co(O/F)_6$ octahedron due to the reduction of the Co/Fe ion by F doping [15]. In summary, lattice expansion due to F doping results from the charge compensation of anions and changes in the structure of the transition metal oxide; this will be discussed in the following XPS result analysis.

The X-ray photoelectron spectroscopy (XPS) peaks displaying the potential-state distributions of elements on the surface of the synthesized LSCFFs are shown in Fig. 2. XPS confirms the presence of F in LSCF, with a characteristic peak at 683.5 eV for F (Fig. 2a). The estimated F content using commercial titration equipment (perfect ION comb F, Mettler Toledo) aligns with the intended ratio (Table S2). Figure 2b and c depict the O 1 s spectra of LSCFF00 and LSCFF05, respectively, deconvoluted into four different peaks corresponding to lattice oxygen species (O_L^{2-}, 528.3 eV), highly oxidative oxygen (O_2^{2-}/O^-, 529.1 eV), surface-absorbed hydroxyl group of oxygen (–OH/O_2, 530.0 eV) species, and surface-adsorbed water species (H_2O, 532.0 eV) [16]. The concentration of highly oxidative oxygen species in LSCFF05 is approximately twice that of LSCFF00, known to improve catalytic OER/ORR properties [17–22]. Based on this result, we can infer that the active oxygen species in the electrochemical reaction increases by F doping. Additionally, the Fe 2p spectra split into two peaks (Fe $2p_{3/2}$ and Fe $2p_{1/2}$) on account of spin – orbit splitting. The Fe $2p_{3/2}$ spectra are fitted with three fitting peaks, as presented in Fig. 2d and e and Table S4, which can be assigned to three types of oxidation states of Fe. As expected from the XRD analysis, the number of reduced Fe oxidation states, Fe^{2+}, increased in LSCFF05 compared to LSCFF00, indicating a significant decrease in the valence of surface Fe cations. This tendency to reduce cations was revealed similarly in cobalt, another B-site element (Fig. S4 and Table S5). As expected, F^-doping primarily reduces the proportion of Fe^{4+} in LSCFF05, weakening the covalency of the M – O bond and facilitating the release of lattice oxygen ions, ultimately leading to the generation of an active surface for OER/ORR [23].

The O_2-temperature programmed desorption (TPD) experiments were conducted to assess the desorption capability of the catalyst for surface oxygen (Fig. 3). Peaks appearing at temperatures below 400 °C are attributed to alpha oxygen (α-oxygen), corresponding to the desorption of surface-physisorbed oxygen, while peaks above 400 °C are attributed to beta-oxygen (β-oxygen) released from the lattice [24]. Alpha oxygen is desorbed from weakly adsorbed

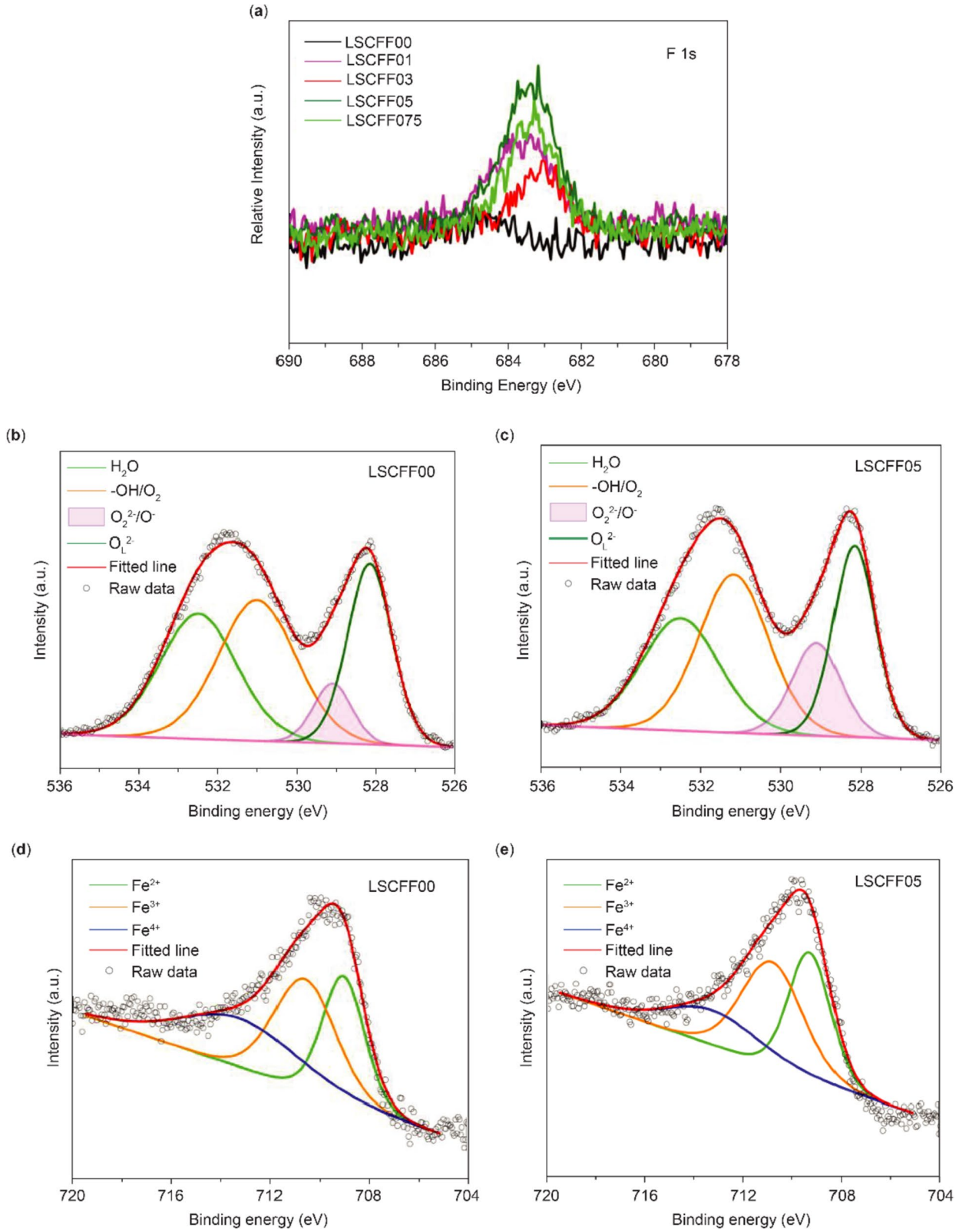

Fig. 2 XPS spectra of **a** F 1 s of LSCFFs and O 1 s of **b** LSCFF00 and **c** LSCFF05. XPS spectra of Fe 2p of **d** LSCFF00 and **e** LSCFF05

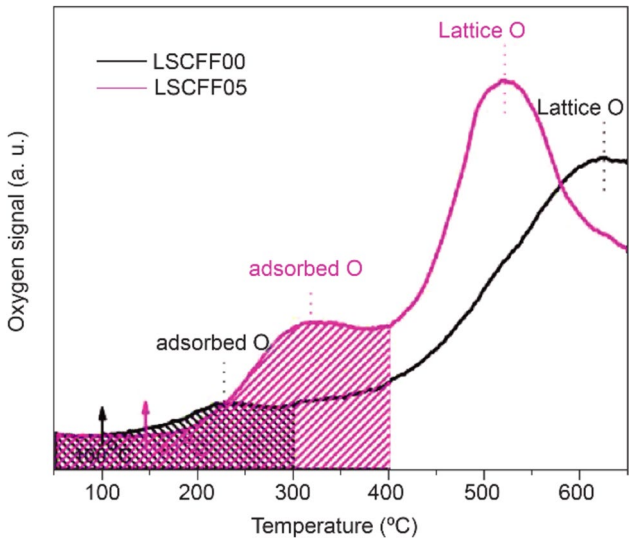

Fig. 3 O_2-TPD profiles of LSCFF00 and LSCFF05

oxygen species on the surface at relatively low temperatures, whereas beta-oxygen originates from tightly bonded lattice oxygen released at high temperatures [25]. In comparison to LSCFF00, LSCFF05 exhibits increased desorption of both physisorbed and lattice oxygen on the surface. The broader peak of adsorbed oxygen at a relatively low temperature indicates that these species can be more easily separated from the surface and can serve as an electrochemical catalyst. This result aligns with the XPS analysis, confirming that the desorption of oxygen generated through F doping is further accelerated, facilitating the movement of oxygen and contributing to OER activity [26].

The electrocatalytic activity of the as-prepared catalyst toward OER/ORR was evaluated in an O_2-saturated 0.1 M KOH electrolyte using Rotating Disk Electrode (RDE). The OER catalytic activity of LSCFF catalysts was then investigated using linear sweep voltammetry (LSV) curves, as shown in Fig. 4a. F doping enhanced OER activity, and among them, LSCFF05 is the most active. In the case of LSCFF05, the onset potential (1.60 V_{RHE}) decreased compared to the sample without doping, LSCFF00 (1.63 V_{RHE}), reducing the potential-gap difference between ORR and OER. Interestingly, the Tafel slope of LSCFF05 (100 mV dec^{-1}), related to the OER reaction rate and activation energy, is lower than that of the commercial OER catalyst, IrO_2 (116 mV dec^{-1}) (Fig. 4b). However, when at the content of F is $x = 0.075$, the activity decreases again, similar to the pattern observed in Xiong's group's BSCF catalyst doped with F. The decrease in OER performance of LSCFF at this composition could be because F would be present in the crystal in excess beyond that, affecting B–O–B bonds, thereby changing the perovskite structure itself. In this case,

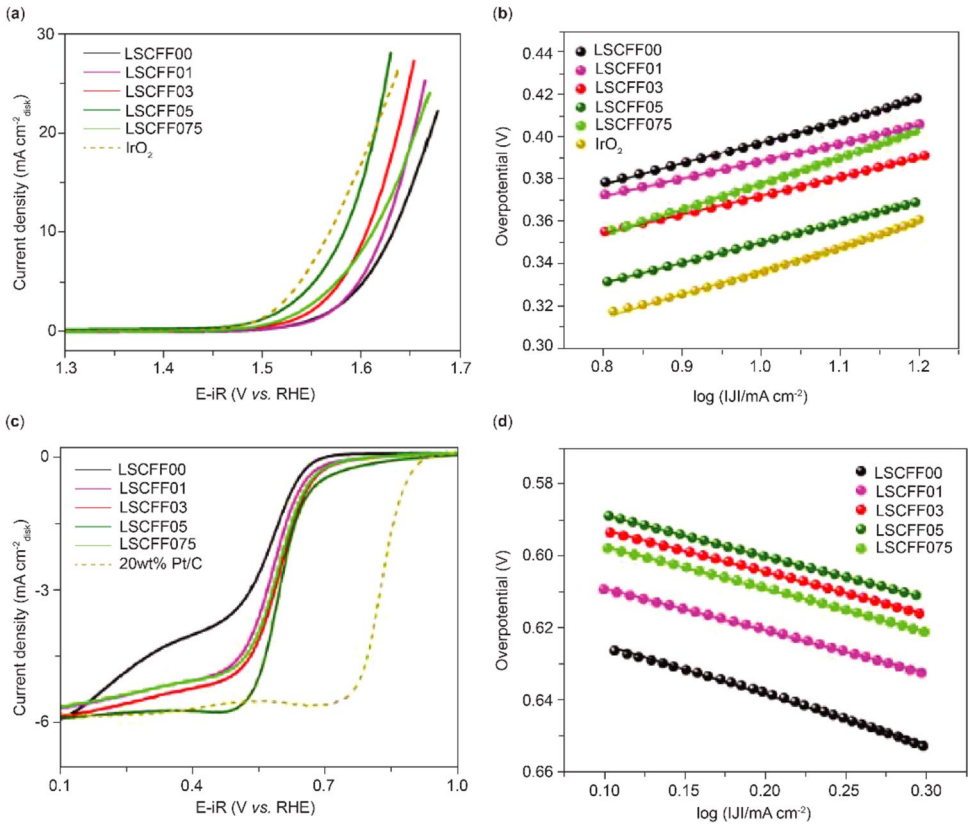

Fig. 4 Catalytic performance of LSCFFs **a** LSV curve for OER, **b** Tafel plot for OER, **c** LSV curve for ORR, and **d** Tafel plot fot ORR

two M-F bonds would replace the M–O–M bond, and there is no B-site cation reduction. [3] Therefore, the decrease in the OER performance above $x = 0.075$ is expected to be due to a decrease in the highly oxidation-active O^{2-}/O^{-} species (Fig. S3). The improved catalytic properties are supported by electrochemical impedance spectroscopy and CV measurements (Fig. S5 and S6). The charge-transfer resistance, associated with the electrochemical reaction rate, is the lowest in LSCFF05 due to the highly increased electrochemically active species such as O^{2-}/O^{-} species. Accordingly, it can be concluded that the OER reaction is accelerated by these species generated by F doping.

The ORR catalyst performance of LSCFFs shown in Fig. 4c was compared with Pt/C, widely used as a commercial ORR catalyst. Although the onset potential of LSCFFs for ORR was not close to that of the precious metal catalyst (Pt/C), the ORR onset voltage positive-shifted as the doping amount increased. The values were 0.52, 0.57, 0.59, 0.58, and 0.58 V_{RHE} for LSCFF00, LSCFF01, LSCFF03, LSCFF05, and LSCFF075, respectively, at 10 mA cm^{2-}. The Tafel slope was also the lowest with the LSCFF05 sample, resulting from the catalytic enhancement attributed to F doping on the oxygen site (Fig. 4d).

Finally, an accelerated degradation test (ADT) for 2,000 cycles was conducted in a potential window encompassing an OER or ORR region (from 0.2 to 1.7 V_{RHE}) to verify the bifunctionality of the catalyst, essential for determining its practical applicability. Additionally, the LSCFF05 sample, which displayed the highest catalytic performance, was measured using the LSV polarization curve data via ADT for 2,000 times and 1,000 times under OER and ORR conditions, respectively. The durability in these electrochemical conditions is also an important factor for applications as a bifunctional catalyst for ORR and OER reactions.

For the durability test, the LSV polarization curve was measured 2,000 times. As shown in Fig. 5a, the initial OER performance of the LSCFF05 sample was lower than that of IrO_2, suggesting that LSCFF05 may be stable under OER conditions. The durability of the LSCFF05 sample under ORR conditions was also confirmed to be stable even after 1,000 consecutive measurements (Fig. 5b). The LSCFF05 sample and a commercial catalyst were applied to homemade Zn-air batteries (Fig. 6 and Fig. S6). The continuous charge/discharge experiment was conducted for approximately 8 h, and despite repeated charge and discharge cycles, when the Zn-air battery was paired with the LSCFF05 catalyst, stable cycle performance was maintained compared to that of the conventional noble catalysts, $Pt/C + IrO_2$. The cycle performance of $Pt/C + IrO_2$ gradually degraded after 50 min, owing to the deterioration of Pt-based catalyst because of dissolution, aggregation, and surface oxidation in alkaline conditions. [27–29] Nevertheless, based on the results that can be compared with that of noble metal catalysts, the

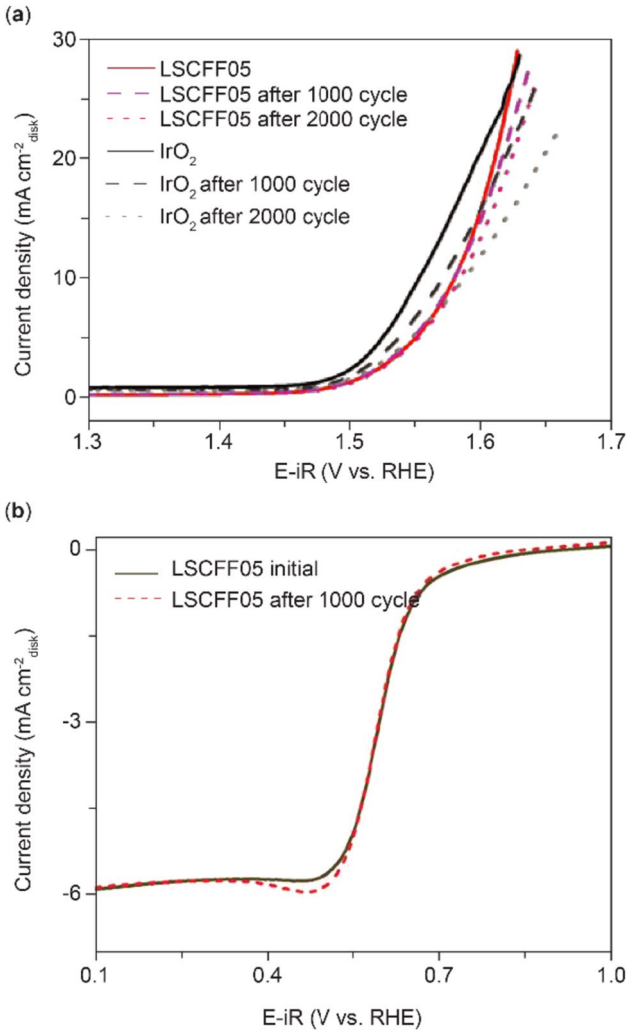

Fig. 5 Stability test **a** LSV polarization curves under OER conditions over 2,000 cycles, and **b** LSV curve under ORR conditions over 1000 cycles

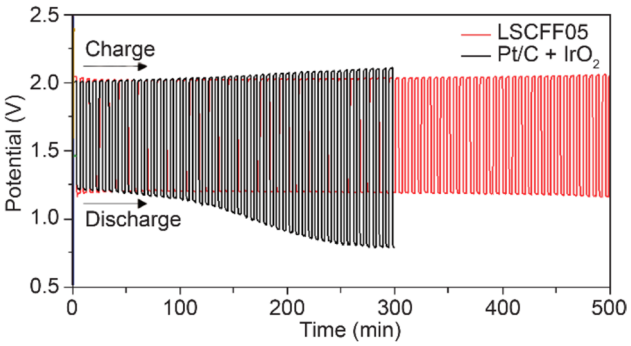

Fig. 6 Cycling performance of zinc-air battery cells with LSCFF05 and Pt/C-IrO_2 mixed cathodes for each cycle of 2 min at 2 mA cm^{-2}

LSCFF05 catalyst can be a candidate extensive bifunctional catalyst for various metal-air batteries, fuel cells, and related electrochemical energy devices.

3 Experimental

The synthesis of fluorine-doped $La_{0.6}Sr_{0.4}Co_{0.2}Fe_{0.8}O_{3-x}$ (LSCFF, $x = 0$, 0.01, 0.03, 0.05, 0.075, and 0.1) denoted as LSCFF00, LSCFF01, LSCFF03, LSCFF05, LSCFF075, and LSCFF10, was conducted via the Pechini method. Stoichiometric amounts of $La(NO_3)_3{\cdot}6H_2O$ (Aldrich, 99 + %), $Sr(NO_3)_2$ (Aldrich, 99 + %), $Co(NO_3)_2{\cdot}6H_2O$ (Aldrich, 98 + %), and $Fe(NO_3)_2{\cdot}6H_2O$ (Aldrich, 98 + %) were dissolved in distilled water, along with corresponding amounts of citric acid and ethylenediaminetetraacetic acid (EDTA), using a stirring bar. The stoichiometry of Sr was adjusted with SrF_2 (Aldrich, 99%) and $Sr(NO_3)_2$. To set the pH value of the solution to 8, $NH_3{\bullet}H_2O$ was added as necessary when all precursors were dissolved. The solution underwent heating to 600 °C for 4 h, resulting in a calcined powder. Subsequently, the obtained powder was sintered at 950 °C in an air-circulated oven. All synthesized powders underwent high-energy ball milling at 450 rpm for 8 h, and dried at 80 °C for 12 h. Under wet-milling conditions, 12.5 ml of ethanol was added to the reactor.

The structures of the synthesized LSCFFs were characterized by X-ray diffraction (XRD) using a Rigaku Ultima IV instrument in Japan. XRD measurements were performed with Cu Kα radiation within a range of $20° < 2\theta < 80°$ and a scan rate of 2.0° min^{-1}. The crystal structures of the synthesized LSCFF samples were determined through the Reitveld refinement method. X-ray photoelectron spectroscopy (XPS) analysis was carried out on the sample surfaces using an Axis-Supra instrument (Kratos) to identify the changes in the chemical states of LSCFFs with increasing fluorine dopants. Additionally, elemental data on the surfaces of the samples were collected using high-resolution transmission electron microscopy (HRTEM; Talos F200X) equipped with an energy-dispersive X-ray (EDX) spectrometer.

A rotating disk electrode (RDE) system (RDE-3A, ALS Co., Ltd) with a potentiostat (VSP-300, Biologic) was employed for measuring the electrocatalytic properties of the LSCFF catalysts at room temperature. To investigate these properties, a standard three-electrode system was utilized, with the electrolyte consisting of 0.1 M KOH solution (pH ~ 13). In the measurement setup, the counter and reference electrodes were a Pt foil and Hg/HgO (saturated 1 M NaOH), respectively. The glassy carbon (GC) with catalyst ink drop-casted was utilized as a working electrode. The catalyst ink was prepared by blending 10 mg of oxide catalyst, 2 mg of Vulcan XC-72r (average particle size 50 nm, Fuel cell store), 100 µl of Nafion solution (5 wt%), and 2 ml of the IPA-water solvent (1:3 v/v). The catalyst suspension underwent ultrasonication for 1 h to homogeneously disperse the catalyst. Subsequently, 4 µl of catalyst ink was drop-casted onto a GC working electrode and dried for 10 min at 60 °C in an air-circulated oven. The mass loading of the catalyst on the working electrode was 0.324 mg_{total} cm^{-2}.

The electrolyte was purged with O_2 gas for 20 min before activity measurement to ensure H_2/H_2O equilibrium at 1.23 V vs. reversible hydrogen electrode (RHE). Prior to collecting linear sweep voltammetry (LSV) data for OER and ORR, cyclic voltammograms (CVs) were obtained at a scan rate of 100 mV s^{-1} until no further change in the curves between cycles was observed. After stabilization, LSV measurements were performed at a rotation speed of 1600 rpm between 0.2 and 0.9 V vs. Hg/HgO (anodic scan) at a scan rate of 5 mV s^{-1} for OER and 0.4 to − 0.9 V vs. Hg/HgO (cathodic scan) for ORR. Electrochemical impedance spectroscopy (EIS) was conducted at 1.61 V_{RHE} under an AC voltage of 5 mV within a frequency range from 100 kHz to 0.1 Hz. iR correction was performed to compensate for any ohmic resistance effects, which were denoted as E-iR (i: current, and R: ohmic resistance measured by high frequency AC impedance). Measured potentials values (vs. Hg/HgO) were calibrated to RHE based on the Nernst equation: $E_{RHE} = 0.0592 \times pH + E_{Hg/HgO} + E_{\text{applied}}$.

The electrochemical performance of the LSCFFs as Zn-air battery catalyst was evaluated using a two-electrode, which comprises a counter electrode, electrolyte, and working electrode. A Zn foil (Alfa Aesar, 99.9%, USA) was utilized for the counter electrode (0.62 mm thick, 1×3 cm^2 in area), and a 6 M KOH solution with 0.2 M zinc acetate served as the aqueous electrolyte. The working electrode was prepared by drop coating the LSCFFs ink with a mass loading of 1 mg cm^{-2} onto a carbon paper with 5 wt% of polytetrafluoroethylene (PTFE) (CNL energy, GDL 10 BCE). The PTFE membrane at the cathode side was employed as the O_2-breathing selective layer for O_2 gas diffusion in ambient air. The reference cathode consisted of commercial 20 wt% Pt/C and IrO_2 powder (in the mass ratio 1:1) (Alfa Aesar, USA). The electrochemical evaluation was conducted using a battery-testing device (WBCS3000, WonATech) at a current density of 2 mA cm^{-2} in a voltage range of 0.5–3.0 V (vs. Zn/Zn^{2+}). Each discharge and charge period was set to be 10 min. The charge/discharge polarization was measured via a current sweep up to 100 mA cm^{-2} (Potentiostat, Zive SP1, WonATech).

4 Conclusions

In this study, powders of $La_{0.6}Sr_{0.4}Co_{0.2}Fe_{0.8}O_{3-x}$ ($x = 0$, 0.01, 0.03, 0.05, 0.075, and 0.1), referred to as LSCFF00, LSCFF01, LSCFF03, LSCFF05, LSCFF075, and LSCFF10,

were synthesized and analyzed for their potential application as a bifunctional electrocatalyst in Zn-air batteries. The findings demonstrate that F doping can enhance the oxygen reduction reaction (ORR) and oxygen evolution reaction (OER) activity, as well as the stability of LSCF catalysts. Notably, the OER performance of the LSCFF05 sample was comparable to that of the state-of-the-art metal catalyst IrO_2. The F-doped LSCF catalyst also exhibited improved cyclic performance for OER/ORR, likely attributed to the increased electrochemically active species resulting from F doping at the oxygen site. This study suggests that the LSCFF05 catalyst holds promise as a potential bifunctional catalyst for various metal-air batteries, fuel cells, and related electrochemical energy devices.

Supplementary Information The online version contains supplementary material available at https://doi.org/10.1007/s13391-023-00483-8.

Funding Open Access funding enabled and organized by KAIST. This research was supported by Ceramic Strategic Technology R&D program through the Korea Institute of Ceramic Engineering & Technology (KICET) (grant NTIS no. 1415187241) and 2022M3H4A1A01008918. This research also has been performed as a cooperation project of "Basic project (referring to projects performed with the budget directly contributed by the Government-funded research Institutes)" and supported by KOREA RESEARCH INSTITUTE of CHEMICAL TECHNOLOGY (KRICT).

Declarations

Conflict of interest There are no conflicts of interest to declare.

References

1. Hong, S., Lee, H., Yu, Y.-S., Park, J., Kim, C.: Development of a rock-salt structure for high energy density lithium-ion batteries. Electron. Mater. Lett. **19**, 359–366 (2023)
2. Kang, C.-Y., Oh, S., Shim, T.Y., Lee, S.-H.: Boosting electrochemical performance of ni-rich layered cathode cia Li2SnO3 surface coating and Sn4+ gradient doping based dueal modification lithium-ion batteries. Electron. Mater. Lett. **19**, 374–383 (2023)
3. Huang, Z.F., Wang, J., Peng, Y., Jung, C.-Y., Fisher, A., Wang, X.: Design of efficient bifuncitional oxygen reduction/evolution electrocatalyst: recent advances and perspectives. Adv. Energy Mater. **7**, 1700544 (2017)
4. Lee, J.S., Kim, S.T., Cao, T., Choi, N.S., Liu, M., Lee, K.T., Cho, J.: Metal-air batteries with high energy density: Li-Air versus Zn-Air. Adv. Energy Mater. **1**, 34–50 (2011)
5. Abraham, K.M.: A polymer electrolyte-based rechargeable lithium/oxygen batteries. J. Electrochem. Soc. **143**(1), 1–5 (1996)
6. Meng, F., Zhong, J., Bao, D., Yan, J., Zhang, X.: In situ coupling of strung Co4N and interwined N-C fibers toward free-standing bifunctional cathode for robust, efficient, and flexible Zn-air batteries. J. Am. Chem. Soc. **6**, 10226–10231 (2016)
7. Zhu, Y., Wang, J., Koketsu, T., Kroschel, M., Chen, J.M., Hsu, S.Y., Henkelman, G., Hu, W., Stasser, P., Ma, J.: Iridium single atoms incorporated in Co_3O_4 efficiently catalyze the oxygen evolution in acidic conditions. Nat. Comm. **13**, 7754 (2022)
8. Ou, G., Yang, C., Liang, Y., Hussain, N., Ge, B., Huang, K., Xu, Y., Wei, H., Zhang, R., Wu, J.: Surface engineering of perovskite oxide for bifunctional oxygen electrocatalysis. Small Methods **3**, 1800279 (2018)
9. Kim, D., Park, J.W., Yun, B.-H., Park, J.H., Lee, K.T.: Correlation of time-dependent oxygen surface exchange kinetics with surface chemistry of $La_{0.6}Sr_{0.4}Co_{0.2}Fe_{0.8}O_{3-d}$ catalysts. ACS Appl. Mater. Interfaces **11**, 31786–31792 (2019)
10. Oh, M.Y., Park, S.K., Park, H., Kim, H., Kang, K., Kim, J.H., Roh, K.C., Shin, T.H.: Enhancement of oxygen reduction reaction catalytic activity via the modified surface of $La_{0.6}Sr_{0.4}Co_{0.2}Fe_{0.8}O_{3-d}$ with palladium nanoparticles as cathode for lithium-air battery. ACS App. Energy Mater. **1**, 5518–5526 (2018)
11. Liu, Y., Wang, W., Xu, X., Veder, J.P.M., Shao, Z.: Recent advances in anion-doped metal oxides for catalytic applications. J. Mater. Chem. A **7**, 7280 (2019)
12. Zhenbao, Z., Yinlong, W., Yijiun, Z., Weim, Z., Zongping, S.: Anion doping: a new strategy for developing high performance perovskite-type cathode materials of solid xode fuel cells. Adv. Energy Mater. **7**, 1700242 (2017)
13. Li, Y., Li, Y., Wan, Y., Zie, Y., Zhu, J., Pan, H., Zheng, X., Xia, C.: Perovskite oxyfluoride electrode enabling direct electrolyzing carbon dioxide with excellent electrochemical performances. Adv. Energy Mater. **9**, 1803156 (2019)
14. Xie, Y., Shi, N., Huan, D., Tan, W., Zhu, J., Zheng, X., Pan, H., Peng, R., Xia, C.: A stable and efficient cathode for fluorine-containing proton-conducting solid oxide fuel cells. Chemsuschem **11**, 3423–3430 (2018)
15. Katsumata, T., Yamamoto, H., Kimura, Y., Amezawa, K., Aso, R., Kikkawa, S., Yamazoe, S., Nakamura, T.: Development of electrochemical anion doping technique for expansion of functional material exploration. Adv. Funct. Mater. **33**, 2307116 (2023)
16. Kim, S., Jung, J.W., Song, D.H., Cho, S.H., Kim, J., Kim, J.K., Oh, D.H., Sun, H., Cho, E.A., Kim, I.D., Jung, W.C.: Exceptionally durable CoFe-exsolved Sr0.95Nb01Co07Fe02O3-d catalyst for rechargeable Zn-air batteries. Appl. Catal. B Environ. **315**, 121553 (2022)
17. Chen, C.F., Kin, G., Dickerson, R.M., Papin, P.A., Gupta, S., Kellogg, S.R., Wu, G.: Oxygen-deficient $BaTiO_{3-x}$ perovskite as an efficient bifunctional oxygen electrocatalyst. Nano Energy **13**, 423–432 (2015)
18. Luo, Z., Miao, R., Huan, T.D., Mosa, I.M., Poyraz, A.S., Zhong, W., Cloud, J.E., Kriz, D.A., Thanneeru, S., He, J., Zhang, Y., Ramprasad, R., Suib, S.L.: Mesoporous MoO_{3-x} material as an efficient electrocatalyst for hydrogen evolution reactions. Adv. Energy Mater. **6**, 1600528 (2016)
19. Wu, R., Zhang, J., Shi, Y., Liu, D., Zhang, B.: Metallic-carbon mesoporous nanowires as highly efficient electrocatalysts for hydrogen evolution reaction. J. Am. Chem. Soc. **137**, 6983–6986 (2015)
20. Bao, J., Zhang, X., Fan, B., Zhang, J., Zhou, M., Yang, W., Hu, X., Wang, H., Pan, B., Xie, Y.: Ultrathin spinel-structured nanosheets

rich in oxygen deficiencies for enhanced electrocatalytic water oxidation. Angew. Chem. **3**, 7507–7512 (2015)
21. Gao, R., Liu, L., Hu, Z., Zhang, P., Cao, X., Wang, B., Liu, X.: The rope of oxygen vacancies in improving the performance of CoO as bifunctional cathode catalyst for rechargeable Li-O2 batteries. J. Mater. Chem. A **3**, 17598–17605 (2015)
22. Li, S.F., Zheng, J., Hu, L., Ma, Y., Yan, D.: Facile surface defect engineering on perovskite oxides for enhanced OER performance. Dalton Trans. **52**, 4207 (2023)
23. Xiong, J., Zhong, H., Li, J., Zhang, X., Shi, J., Cai, W., Qu, K., Zhu, C., Yang, Z., Beckman, S.P., Cheng, H.: Engineering highly active oxygen sites in perovskite oxides for stable and efficient oxygen evolution. Appl. Catal. B **256**, 117817 (2019)
24. Yang, C., Tian, Y., Pu, J., Chi, B.: Anion fluorine-doped $La_{0.6}Sr_{0.4}Fe_{0.8}Ni_{0.2}O_{3-\delta}$ perovskite cathodes with enhanced electrocatalytic activity for solid oxide electrolysis cell direct CO_2 electrolysis. ASC Sustainable Chem. Eng. **10**, 1047–1058 (2022)
25. Yuan, Y., Wang, J., Adimi, S., Shen, H., Thomas, T., Ma, R., Attfield, J.P., Yang, M.: Zirconium nitride catalysts surpass platinum for oxygen reduction. Nat. Mater. **19**, 282–286 (2020)
26. Kayaalp, B., Lee, S., Klauke, K., Seo, J., Nodari, K., Kornowski, A., Jung, W.C., Mascotto, S.: Template-free mesoporous $La_{0.3}Sr_{0.7}Ti_{1-x}Fe_xO_{3\pm\delta}$ for CH_4 and CO oxidation. Appl. Catal. B Environ. **245**, 536–545 (2019)
27. Huang, X., Zhao, Z., Cao, L., Chen, Y., Zhu, E., Lin, Z., Li, M., Yan, A., Zettl, A., Wang, Y.M., Duan, Z., Mueller, T., Huang, Y.: High-performance transition metal-doped Pt_3Ni octahedra for oxygen reduction reaction. Science **348**, 1230–1234 (2015)
28. Li, M., Zhao, Z., Cheng, T., Fortnelli, A., Chen, C.-Y., Yu, R., Zhang, Q., Gu, L., Morinov, B.V., Lin, Z., Zhu, E., Yu, T., Jia, Q., Guo, J., Zhang, L., Goddard, W.A., III., Huang, Y., Duan, Z.: Ultrafine jagged platinum nanowires enable ultrahigh mass activity for oxygen reduction reaction. Science **356**, 1414–1419 (2016)
29. Suk, J.H., Hwang, N.M.: Non-classical crystallization of bulk crystals in solution and of thin films in the gas phase by chemical vapor deposition. Electron. Mater. Lett. **18**, 1–26 (2022)